8-17-2018

A Study of Hα Line Profile Variations in β Lyr

Richard Ignace
East Tennessee State University, ignace@etsu.edu

Sharon K. Gray
East Tennessee State University

Macno A. Magno
East Tennessee State University

Gary D. Henson
East Tennessee State University, hensong@etsu.edu

Derek Massa
Space Science Institute

Citation Information

Ignace, Richard; Gray, Sharon K.; Magno, Macno A.; Henson, Gary D.; and Massa, Derek. 2018. A Study of Hα Line Profile Variations in β Lyr. *The Astronomical Journal*. Vol.156(97). https://doi.org/10.3847/1538-3881/aad339 ISSN: 0004-6256

A Study of Hα Line Profile Variations in β Lyr

The Astronomical Journal, 156:97 (12pp), 2018 September https://doi.org/10.3847/1538-3881/aad339

A Study of Hα Line Profile Variations in β Lyr

Richard Ignace[1], Sharon K. Gray[1], Macon A. Magno[1], Gary D. Henson[1], and Derck Massa[2]
[1] Department of Physics and Astronomy, East Tennessee State University, Johnson City, TN 37663, USA; ignace@etsu.edu
[2] Space Science Institute, 4750 Walnut Street, Suite 205, Boulder, CO 80301, USA
Received 2018 June 8; revised 2018 July 9; accepted 2018 July 10; published 2018 August 17

Abstract

We examine over 160 archival Hα spectra from the Ritter Observatory for the interacting binary β Lyr obtained between 1996 and 2000. The emission is characteristically double-peaked, but asymmetric, and with an absorption feature that is persistently blueshifted. Using a set of simplifying assumptions, phase varying emission line profiles are calculated for Hα formed entirely in a Keplerian disk, and separately for the line formed entirely from an off-center bipolar flow. However, a dynamic spectrum of the data indicates that the blueshifted feature is not always present, and the data are even suggestive of a drift of the feature in velocity shift. We explore whether a circumbinary envelope, hot spot on the accretion disk, or accretion stream could explain the observations. While none are satisfactory, an accretion stream explanation is somewhat promising.

Key words: accretion, accretion disks – binaries: eclipsing – binaries: visual – stars: early-type – stars: individual (β Lyr)

1. Introduction

β Lyr is a well-studied yet complex massive, interacting, eclipsing binary star (Sahade 1980; Hubeny et al. 1994; Harmanec 2002). Basic parameters of the system adopted for our study are given in Table 1, indicating two B-star components in a 12.9 day period with a circular orbital separation of $a \approx 55\,R_\odot$, and an accretion disk with a radius of $R_D \approx 30\,R_\odot$. The deeper minimum occurs when the less massive more luminous giant star is eclipsed. This giant star will hereafter be referenced as the "Loser" star, and the more massive component will be the "Gainer" star. The binary has been heavily studied in the radio (e.g., Wade & Hjellming 1972; Jameson & King 1978; Umana et al. 2002), infrared (e.g., Knappenberger & Fredrick 1968; Alduseva & Esipov 1969; Jameson & Longmore 1976; Zeilik et al. 1982), optical (e.g., Harmanec et al. 1996; Schmitt et al. 2009; Bonneau et al. 2011; Rucinski et al. 2018), ultraviolet (e.g., Hack et al. 1975; Mazzali 1987; Kondo et al. 1994), and X-ray (e.g., Mewe et al. 1976; Ignace et al. 2008) bands. The system has also been a frequent target for polarimetric studies (e.g., Appenzeller & Hiltner 1967; Hoffman et al. 1998; Lomax et al. 2012). It is unusual for its geometrically and optically thick disk enveloping an unseen "primary"[3] (Huang 1963; Wilson 1974; Hubeny & Plavec 1991; Zhao et al. 2008) and bipolar "jet-like" outflow (Harmanec et al. 1996; Hoffman et al. 1998). Even the detection and dynamical influence of a magnetic field has been claimed (e.g., Skulskij 1982; Leone et al. 2003). With such rare physical features and a near-edge-on view, β Lyr has been the subject of considerable modeling, including hydrodynamic simulations (e.g., Bisikalo et al. 2000; Nazarenko & Glazunova 2003, 2013), complex stellar wind scenarios (Mazzali et al. 1992), the accretion disk modeling (e.g., Linnell 2000, 2002), and the evolutionary state of the binary (Mennickent & Djurašević 2013).

Our study focuses on β Lyr's Hα emission line. The Hα line of β Lyr has proven to be an important feature in studies of the binary. Interferometric studies of Hα emission were a leading indicator of the bipolar outflow in the binary system (Harmanec et al. 1996) and continue to be used in such approaches. Sanyal (1976) used a set of observations of Hα to consider relatively rapid variations on minutes and hours (as compared to the 12.9 day period) to interpret these effects in terms of hot spots associated with the accretion flow onto the Gainer's disk. Huang (1978) focused on the asymmetry in the double-peaked Hα line profile shape, and the persistent blueshifted absorption feature in the line to propose a model involving both expansion and rotation. Honeycutt et al. (1993) obtained 52 spectra that were used to create a "dynamic spectrum" in which spectra were binned and grouped in 13 phase intervals to produce a grayscale representation of the varying emission profile. While the authors comment that previous studies interpreted the line shape in terms of a rotating wind (Etzel & Meyer 1983) or a thick disk and circumbinary shell (Batten & Sahade 1973), Honeycutt et al. (1993) use their dynamic spectrum to suggest that β Lyr bears similarity to cataclysmic variable systems. Ahmad & Zainuddin (2009) discuss Hα in terms of V/R variation, where "V" refers to the blueshifted peak intensity and "R" refers to the redshifted one. Their study uses data from the University of Toledo's Ritter Observatory (from 1999 June to September) supplemented with data from the Langkawi National Observatory in 2007.

For our contribution to the subject, we employ a larger data set from the archive at the Ritter Observatory, as described in Section 2. Models involving a Keplerian disk and an off-center bipolar flow are described in Section 3. A phase-sequenced dynamic spectrum based on the Hα data is given in Section 4 to interpret what appears to be the cyclical appearance and absence, along with a drift, in the absorption component that is seen only at blueshifted velocities. Concluding remarks are given in Section 5, and the Appendix includes details about coordinate systems used in the modeling.

[3] Here "primary star" refers to the more massive component of the binary, even though the light-curve minimum in the optical occurs when the secondary star is eclipsed.

Table 1
System Parameters for β Lyr

Identifiers	Sheliak; HD 174638; HR 7106
d (pc)	295 ± 15
$P_{\rm orb}$ (days)	12.9
$\Omega_{\rm orb}$ (Hz)	5.64×10–6
a ($R_\odot$)	55
a_1 ($R_\odot$)	10.
a_2 ($R_\odot$)	45
$v_{\rm orb,1}$ (km s^{-1})	40.
$v_{\rm orb,2}$ (km s^{-1})	175
i (°)	86
R_D ($R_\odot$)	30

2. Observations of β Lyr

The Ritter Observatory[4] operates a 1.06 m reflector, employing an echelle spectrograph with a resolving power of 26,000 at Hα (corresponding to a velocity resolution of 11.5 km s^{-1}). We retrieved 169 CCD spectra of β Lyr from the public archive maintained by the Observatory. These spectra span a period between 1993 and 2000. For our study, we used 162 spectra taken between 1996 and 2000 (see Table 2). Seven spectra were omitted from this study as they were inappropriate for analysis. Typically, a single spectrum was obtained each night. However, multiple spectra (from 2 to 6) were acquired in rapid succession on eight nights in 1997, twice in 1998, and once in 2000.

The data are stored in fits files that are stacked in nine echelle orders between the 5285 and 6595 Å wavelengths. Our study is based on isolating the Hα (6562.8 Å) emission line that is in the ninth order. Interactive Data Language software routines were used to extract the Hα data for each of the 162 spectra.

With a focus on Hα, we selected a range of the wavelengths centered on this line and performed a linear least squares fit using points free of spectral lines to determine a continuum level. Examples of the continuum-normalized emission profiles are shown in Figure 1. The profile is characteristically double-peaked but strongly asymmetric. Line equivalent widths vary significantly, by a factor of about 3. However, the variation is largely anticorrelated with the optical light curve (e.g., Gray & Ignace 2008). Peak emission in the continuum-normalized profile typically achieves a value of 2–3, but can rise as high as 6. The half-width at half-maximum (HWHM) is ~200 km s^{-1}, although the wings of the line can extend to twice that.

The time of each observation was converted to heliocentric Julian date (HJD). The phase of each observation was calculated using the quadratic ephemeris equation of Harmanec & Scholz (1993):

$$T = T_0 + T_1\, E + T_2\, E^2, \tag{1}$$

where $T_0 =$ HJD 2408247.966, $T_1 = 12.913780$ days represents the binary period at T_0, and $T_2 = 3.87196 \times 10^{-6}$ days represents the period change. Sampling of the archival data is given in Figure 2, with the upper panel showing points at which data were taken as a modified HJD, given by subtracting 2449261. The lower panel provides a histogram to illustrate the

[4] See astro1.panet.utoledo.edu/~wwwphys/ritter/ritter.html for further technical details.

Table 2
Journal of Observations

Year	Months	# of Spectra
1996	August	2
1997	April–November	74
1998	April–October	29
1999	June–September	41
2000	August–September	15

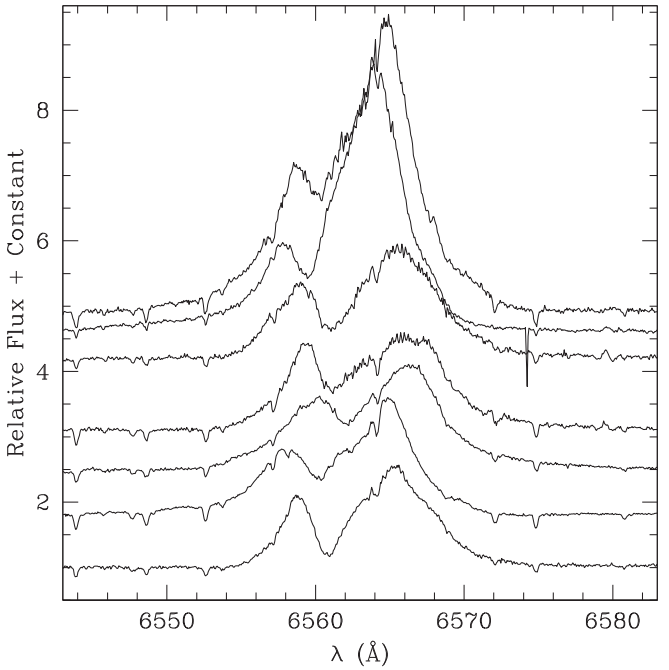

Figure 1. Selection of continuum-normalized Hα emission line profiles from the Ritter Observatory's public archive. Each profile has been shifted vertically for better ease of viewing.

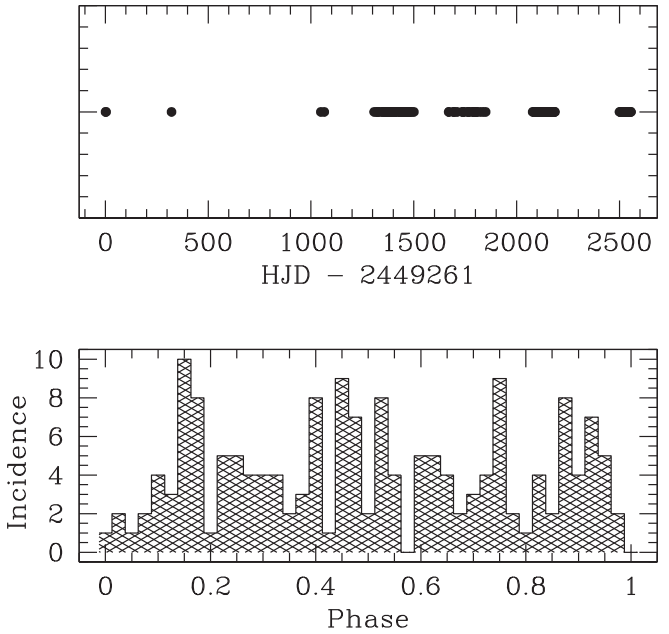

Figure 2. Upper panel shows the sampling of spectra obtained over a modified heliocentric Julian Date. Lower panel indicates the sampling of spectra after dates were phased on the binary orbit (see the text).

Table 3
Parameters for β Lyr Stellar Components

	Gainer	Loser
Sp. Type	B0V/B1V	B8III/B8II
$T_{\rm eff}$ (K)	32,000	13,300
M ($M_\odot$)	13	3
R ($R_\odot$)	6	13
L (10^4 $L_\odot$)	34,000	4700
$v_{\rm rot}$[a] (km s^{-1})	24	51

Note.
[a] Equatorial rotation speeds assuming synchronous rotation and no oblateness.

sampling in orbital phase, based on Equation (1), with bin widths of 0.025 in phase.

3. Line Profile Modeling

The β Lyr system is a complex multicomponent system consisting at minimum of two stars, an accretion disk, a bipolar outflow that is offset from either star, an accretion stream, and a "hot spot" where the accretion stream merges with the disk. There is even evidence for a circumbinary envelope. Table 3 lists stellar parameters adopted for use in this study, in conjunction with system parameters from Table 1. For Table 3, the notation for stellar properties is standard. Note that the spectral types are debatable, especially the Gainer star obscured by the accretion disk. The last row of the table gives equatorial rotation speeds of the stars assuming synchronous rotation. Both values are small compared to the critical speeds of break-up, so neither component is considered rapidly rotating. Note that in the modeling that follows, the system is so close to edge-on, at 86° or possibly greater (see Table 1), that illustrative results will assume an inclination of $i = 90°$ for simplicity.

For illustration, Figure 3 displays the Roche potential for the system with the Gainer (blue), Loser (magenta), and disk (green) parameters overplotted. Isopotential values were selected to yield somewhat regularly spaced contours in the orbital plane defined by the barycenter (hence the "b" subscription; see the description of coordinate systems below). Based on this figure, it is reasonable that the Gainer is spherically symmetric and that much of the disk can be approximated as axisymmetric. The approximation of sphericity is less secure for the Loser star, but will be adequate for our purposes.

In order to model the system, it is important to have several coordinate systems to relate to the various components and how the components move with orbital phase. Detailed descriptions for coordinate transformations are provided in the Appendix. The following highlights the principle systems and considerations.

1. *Observer Coordinates:* Cartesian coordinates (x, y, z) are situated such that the origin is the barycenter of the binary, an observer is along the $+z$-axis, and the y-axis is parallel with the orbital angular momentum of the binary as projected in the sky. For example, if the binary were exactly edge-on, the observer y-axis would coincide with the axis of revolution for the binary, at the barycenter. Then the x-axis is defined by $\hat{x} = \hat{y} \times \hat{z}$. Spherical coordinates for the observer are (r, θ, α), and cylindrical coordinates are (p, α, z), where p is an impact parameter in the plane of the sky. Figure 4 presents a top-down view of the orbital plane with the Gainer, Loser, and accretion disk shown to scale (according to parameters in Table 1). Here "b" is the barycenter. An observer direction is indicated at an orbital phase of $\epsilon \approx 1/6$ (zero phase would place the Loser directly behind the Gainer from the observer's point of view). Here, ϵ is the variable for phase that ranges from 0 to 1. A position for the center of the jet

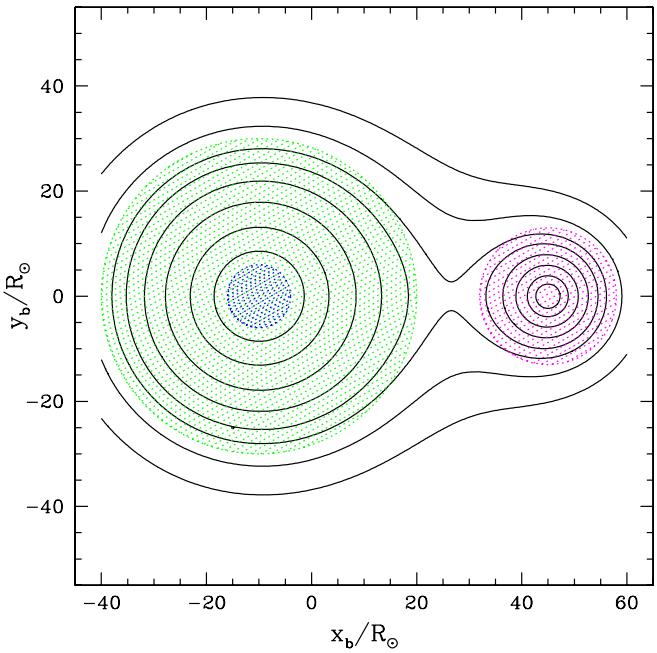

Figure 3. Contours for the Roche potential in the orbital plane. Coordinates are in the barycenter system of (x_b, y_b, with the barycenter at (0, 0)). Values are in terms of $R_\odot$. The Gainer star is blue; the Loser is magenta; the disk is green. All three are assumed axisymmetric. Sizes are taken from Tables 1 and 3.

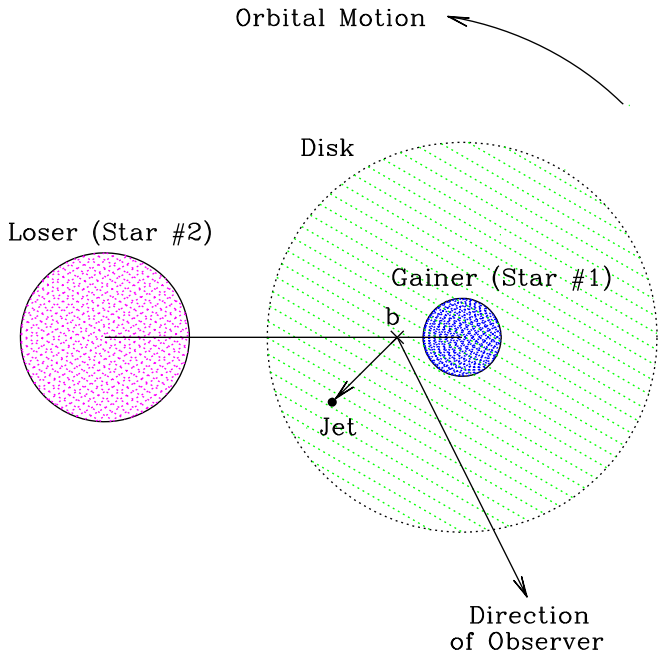

Figure 4. Top-down view of the binary orbit with two stars and disk shown to scale. The cross marked "b" is the barycenter for the adopted properties of the stars. The dot marked "J" represents the origin for the jet, as originating from somewhere in the disk. The observer direction is indicated for an arbitrary phase in the orbit.

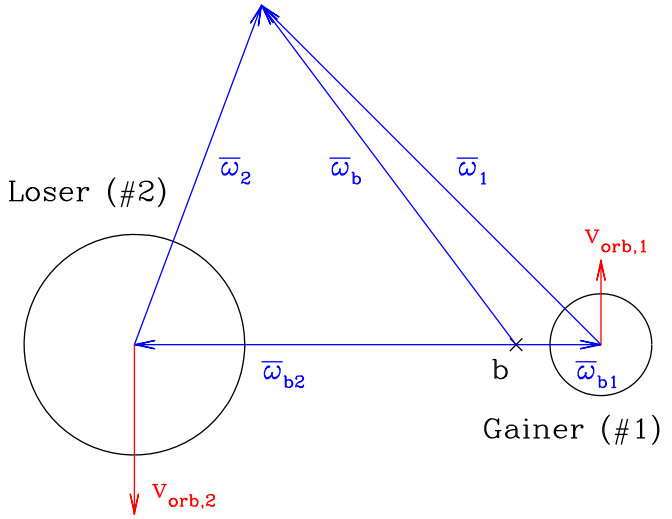

Figure 5. Top-down view of the orbital plane indicating the relationship between different coordinates, where ϖ is a cylindrical radius. Also indicated are orbital velocities of the stellar components. The sizes of the stars, their spacing, and the location of the barycenter (indicated by "b") are all to scale.

is given by way of illustration; its exact location is not known.

2. *Binary Coordinates:* With the barycenter at the origin of the system, Cartesian coordinates for the binary are (x_b, y_b, z_b). In this system, z_b is the axis of revolution for the binary orbit. By convention, primary eclipse occurs when the Loser star is at the rearside of the disk. This corresponds to orbital phase $\epsilon = 0$. We take the position of the Loser to be

$$x_{b,2} = a_2 \cos(\Omega\, t), \tag{2}$$

$$y_{b,2} = a_2 \sin(\Omega\, t), \tag{3}$$

$$z_{b,2} = 0; \tag{4}$$

and the Gainer star to be

$$x_{b,1} = a_1 \cos(\Omega\, t + \pi), \tag{5}$$

$$y_{b,1} = a_1 \sin(\Omega\, t + \pi), \tag{6}$$

$$z_{b,1} = 0. \tag{7}$$

With these definitions, the orbital phase tracks with the azimuth of the Loser star, $\varphi_{b,2}$, $\epsilon = \varphi_{b,2}(t)/2\pi$.

Spherical coordinates in the barycenter system are (r_b, ϑ_b, φ_b), and cylindrical coordinates are (ϖ_b, φ_b, z_b).

3. *Stellar Coordinates:* Notation for the star coordinates follow those for the barycenter, but with subscripts of "1" for the Gainer and "2" for the Loser. The orientation of the Cartesian coordinates for the three systems have all of the x, y, and z axes similarly oriented. For example, $+z_b$, $+z_1$, and $+z_2$ are all parallel. If $x_{b,1} = -a_1$ and $x_{b,2} = +a_2$, then the x_1-coordinate for the barycenter is $+a_1$, and the x_2-coordinate is $-a_2$. Figure 5 provides an illustration of the relative positioning of cylindrical radii for the barycenter, Gainer, and Loser systems. The three vectors in the upward direction in the figure are for an arbitrary point in the orbital plane. Also indicated are the instantaneous orbital velocity vectors of the stars (values given in Table 1).

Note that the accretion disk is centered on the Gainer star, and so the coordinates for the disk are conveniently defined in the Gainer star system.

4. *Jet Coordinates:* The last system is the jet itself. When calculating line profile shapes for the jet component, it will prove convenient to define properties such as density and velocity in the jet system, and then use coordinate transformations to the observer system.

The jet is taken to be a biconical outflow, where the vertex is in the orbital plane, with symmetry axis normal to that plane. Cartesian coordinates in the jet system are (x_J, y_J, z_J), where z_J is the symmetry axis of the cone. The x-axis for the jet corresponds to the outward cylindrical radial from the Gainer star, which in unit vectors is $\hat{x}_J = +\hat{\varpi}_{2,J}$. Spherical and cylindrical coordinates in the jet system follow that of the barycenter and the two stars.

3.1. Line Profiles from the Disk

3.1.1. Theory

An axisymmetric, rotating circumstellar disk can generally be expected to produce emission line profiles that are double-peaked in shape (e.g., Horne & Marsh 1986). The objective of our modeling is to obtain qualitative features for Hα emission produced in the disk, and to simulate how the profile shape varies with orbital phase. This involves modeling not only the line formation throughout the disk, but also attenuation by the continuous opacity of the thick disk, plus the effect of eclipse by the Loser star. Loosely following Rybicki & Hummer (1983), we use the Sobolev theory (Sobolev 1960) for an edge-on disk in Keplerian rotation.

The disk is taken to be axisymmetric with a density profile described most conveniently in the stellar coordinates of the Gainer, as given by

$$\rho(\varpi_1, z_1) = \rho_0\, e^{-|z_1|/H_D}\, e^{-\varpi_1^2/R_D^2}, \tag{8}$$

where ρ_0 is a constant that is set by the total mass in the disk. Estimates for the dimensions of the disk are $R_D \approx 5R_1$ and $H_D \approx R_1$. The density has an exponential vertical decline, but a Gaussian decline in cylindrical radius. The latter serves to rather rapidly truncate the radial extent of the disk.

The Gainer star has a critical speed of rotation at its equator of

$$v_{c,1} = \sqrt{\frac{GM_1}{R_1}} \approx 640 \text{ km s}^{-1}. \tag{9}$$

Hereafter, it is convenient to normalize lengths to the radius of the Gainer. The Keplerian rotation in the disk (taken as uniform with height in the slab) is

$$v_K(\varpi) = v_{c,1} \sqrt{\frac{1}{\varpi}}. \tag{10}$$

The Doppler shift with respect to a distant observer is

$$v_z = \boldsymbol{v}_K \cdot \hat{z} + \boldsymbol{v}_{\rm orb} \cdot \hat{z}, \tag{11}$$

where the second term represents an additional velocity shift owing to the participation of the disk in the binary orbit about the barycenter. The disk is assumed stationary in the corotating frame. As a result, in the observer frame, locations in the disk have a Doppler shift arising from solid body rotation about the

barycenter. The observed velocity shift becomes

$$v_z = v_{c,1}\,\frac{\sin\varphi_1}{\sqrt{\varpi}} + \Omega\, R_1\, \varpi_b \sin\varphi_b. \tag{12}$$

The critical speed of rotation for the Gainer is about 640 km s^{-1}. The outer edge of the disk rotates with a Keplerian speed of 290 km s^{-1}. The maximum solid body rotation speed in the disk, relative to the barycenter, is 160 km s^{-1}. While 160 km s^{-1} is nontrivial compared to the slowest Keplerian speed in the disk, much of the disk has a solid body rotation that is considerably smaller than the Keplerian speed. As a result, we model disk line profiles based on Sobolev theory for a disk with no solid body rotation, and then include a shift of the resulting profile as a whole with an amplitude that mimics that of the Gainer star's radial velocity shift, with respect to the barycenter. The consequence of this simplification is that, in the absence of an eclipse by the Loser, our disk line profiles are left–right symmetric about a bisector. With solid body rotation, we would expect a double-peaked line shape that is slightly asymmetric in a phase-dependent way, owing to how the solid body rotation term generally produces a differential distortion of the isovelocity zones between the blue- and redshifted sides. (Note that the phase-averaged line profile would still be symmetric about line center.)

Following Rybicki & Hummer (1983), the Sobolev optical depth is given by

$$\tau_S = \mathcal{T}_L \left(\frac{\rho}{\rho_0}\right)^2 \frac{\varpi_1}{2\,|w_z|\,\sqrt{1 - \varpi_1\, w_z^2}}, \tag{13}$$

where $\mathcal{T}_L$ is a free parameter for the scaling of the line optical depth, ρ_0 is the peak density in the disk, the square of density is a scaling appropriate for modeling Hα as a recombination line. The normalized line-of-sight Doppler velocity shift in the profile is w_z for emission arising in the disk. It is normalized to the critical speed of rotation for the Gainer star and is given by

$$w_z = v_{\varphi,1}/v_{c,1} = \frac{\sin\varphi_1}{\sqrt{\varpi_1}}, \tag{14}$$

where $v_{\varphi,1}$ is the Keplerian azimuthal speed is the disk. Consequently, w_z ranges from -1 to $+1$ for this case.

An isovelocity zone is a volume in the disk for which w_z is a constant. An example of such zones can be found in Ignace (2010; Figure 2 of that paper). The contour for constant w_z is a dipole-like loop with inner radius $\varpi = 1$ at the surface of the Gainer star, and outer radius $\varpi_{max}(w_z) = 1/w_z^2$.

An unocculted edge-on disk is for simplicity taken to produce a specific flux of continuum emission given by:

$$f_D = \frac{2H_D \cdot 2R_D}{d^2} \cdot S_D \int_0^\infty (1 - e^{-\tau_D})dp, \tag{15}$$

where d is distance to the star, τ_D is the disk optical depth, $2H_D$ is from the vertical integral through the disk, and S_D is the source function in the disk, here taken as a constant. Another factor of two appears because the integration limits are for just half of the disk. Note that for an edge-on disk with $\tau_D \gg 0$, the flux becomes $f_D \approx (\sqrt{\pi}\, H_D\, R_D/d^2) S_D$.

The disk optical depth is expressed as

$$\tau_D = 2\mathcal{T}_C\, e^{-p^2/R_D^2}. \tag{16}$$

Here $2\mathcal{T}_C$ is the total optical depth along a diameter through the disk, as if the Gainer star were not present. For convenience the product of opacity and density as integrated along a chord in the orbital plane is here assumed to yield a Gaussian dependence with the observer's impact parameter, p.

The specific flux of line emission at w_z is given by

$$f_L(w_z) = 2H_D\, R_1 \int_1^{\varpi_0(w_z)} S_L(1 - e^{-\tau_S}) \times \frac{3}{2}\, w_z\, \varpi_1\, \Lambda(\varpi_1, w_z) d\varpi_1, \tag{17}$$

where S_L is the line source function, and the appearance of $2H_D$ indicates that the result for the midplane of the disk applies for every height in the disk slab.

The factor Λ accounts for the attenuation of line photons by the continuous opacity of the optically thick disk. The isovelocity zones for an axisymmetric, rotating disk are left–right symmetric. The disk rotates counterclockwise as seen from above, so blueshifts arise on the left side for an observer, and redshifts on the right side. A single isovelocity contour is a loop, and therefore has a front-side branch and backside branch. The extinction of line photons on the near branch is less than for the back.

The factor Λ is given by

$$\Lambda = e^{-\tau_{D,A}}\, e^{-\tau_S} + e^{-\tau_{D,B}}. \tag{18}$$

where A and B are, respectively, for the near and far branches, and the additional factor relating to the Sobolev optical depth is a recognition that line photons produced in the far branch are also attenuated by the line opacity in the near branch (Rybicki & Hummer 1978). Note that for an optically thin line and optically thin disk, $\Lambda \approx 2$. This is because the flux integral is for just the near branch, but both front and rear contribute to the line at normalized velocity shift w_z. If the disk is extremely thick, $\Lambda \to 0$.

3.1.2. Results

Given the prescribed geometry of the disk, and treating the system as viewed edge-on, the main free parameters of the model are $\mathcal{T}_L$ to control the line strength, $\mathcal{T}_C$ to control the severity of disk extinction, S_L for the line source function, and S_D for the disk source function. In addition, we assume that at Hα, the line source function scales as a blackbody in the Rayleigh–Jeans (RJ) limit at isothermal temperature $T_L = 20{,}000$ K. For S_D, the disk is taken to emit like a blackbody of temperature $T_D = 9000$ K, also in the RJ limit.

Figure 6 illustrates profile shapes for a range of different optical depth combinations. Panels (a) through (d) are for $\mathcal{T}_C = 0.3$, 1.0, 3.0, and 10.0, respectively. In each panel, the four line profiles are for $\mathcal{T}_L = 0.3$, 1.0, 3.0, and 10.0, with stronger lines resulting for larger $\mathcal{T}_L$ values. All the line profiles are displayed as continuum normalized. In these examples, the Loser star is at orbital phase 0.0, so there is no eclipse of either the Loser or the disk, to influence either the profile shape or the continuum normalization. The normalization takes into account flux from the Loser star and the disk, including generally when either the Loser or the disk are in eclipse.

The profiles are mainly illustrative. They demonstrate that for an axisymmetric disk there is a line shape that is double-peaked and symmetric about line center results. When the line

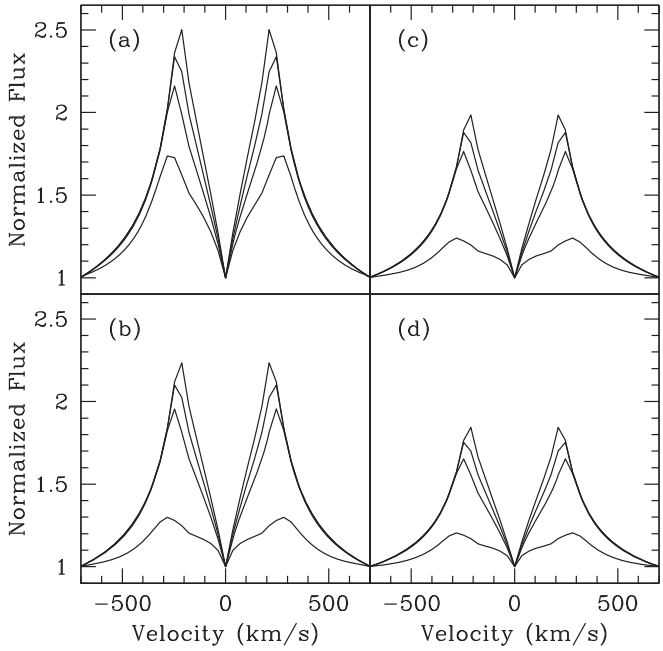

Figure 6. Series of model line profiles formed in the Keplerian accretion disk. Each panel has four line profiles, with $\mathcal{T}_L = 0.3$, 1.0, 3.0, and 10.0. The different panels are for different optical depths in the disk, with $\mathcal{T}_C = 0.3$, 1.0, 3.0, and 10.0 for panels (a)–(d), respectively.

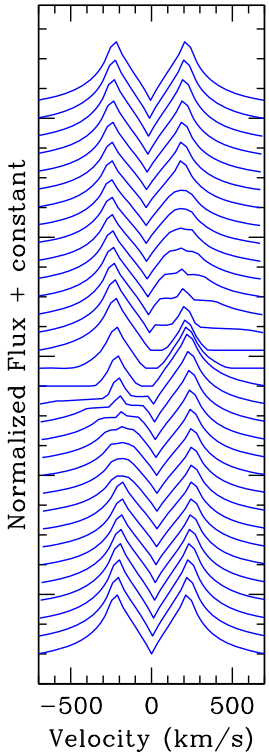

Figure 7. Series of disk line profiles with orbital phase for $\mathcal{T}_L = 10.0$ and $\mathcal{T}_C = 3.0$. The profiles are vertically offset by a constant for ease of viewing, with phase $\epsilon = 0$ at the bottom and $\epsilon = 1$ at the top. There are 33 profiles shown. The phase interval between profiles is $\Delta\epsilon \approx 0.03$. The distortion to the profiles around ϵ of 0.5 arises from an eclipse of the disk by the Loser, which first affects the blueshifted side, then the redshifted side.

is optically thick, a distinct wedge-shaped central depression results. When the line is more optically thin, the central depression has more structure. Rybicki & Hummer (1983) considered rotating rings and found a range of profile morphologies from "M" shapes for thick lines to "U" shapes for thin ones. Our construction, based on their approach, is a series of nested rings, each having its own optical depth, but modified according to absorption by continuous opacity of the disk.

A few interesting points. (1) The peaks are less separated as $\mathcal{T}_L$ increases. (2) Peak emission is overall depressed as $\mathcal{T}_C$ increases. Note that none of these examples achieve peak values as large as the observed maximum. With a disk that is essentially truncated, increasing $\mathcal{T}_L$ has limits for increasing the line emission. At some point the only way to obtain a stronger line is to increase S_L. (3) While the line peaks extend to $\approx \pm 300\,\mathrm{km\,s^{-1}}$ (somewhat higher values than observed), the emission wings can go to rather large values, beyond $\pm 500\,\mathrm{km\,s^{-1}}$. The highest speed line emission originates from close to the star, where Keplerian rotation is greatest. The maximum Keplerian speed is $640\,\mathrm{km\,s^{-1}}$ at $\varpi_1 = 1$ (i.e., radius of the Gainer star).

Figure 7 shows a series of disk profiles as a function of orbital phase. Each profile is shifted vertically for ease of viewing. The profile at the bottom is for phase $\epsilon = 0.0$; the topmost is for $\epsilon = 1.0$. The development of asymmetry at middle phases, around $\epsilon = 0.5$, arises when the Loser eclipses the disk. The eclipse first affects the blueshifted velocities, and then migrates across to redshifted ones. In these examples, a significant fraction of the line emission can be blocked, but the continuum normalization also evolves, because the disk is being eclipsed.

3.2. Line Profiles from the Jet

3.2.1. Theory

To model emission line profiles from a jet, Sobolev theory is again employed; however, the geometry and velocity field are quite different from the disk case. The jet is approximated as a biconical flow, with center situated in the disk. We again assume that the system is viewed edge-on. Next we treat the biconical flow as being a portion of a spherical wind. In other words, the velocity and density in the flow are functions only of radius from the vertex of the cone, r_J: the density producing Hα is nonzero within the biconical of half-opening angle β_J and zero outside of it.

For the velocity field, the flow is assumed to expand homologously, with no rotation, with

$$v(r_J) = v_0\left(\frac{r_J}{R_1}\right), \tag{19}$$

where R_1 is used to normalize the radius, and v_0 is a scale parameter for the velocity. Mass continuity provides the density in the jet, with

$$\rho(r_J) = \frac{\dot{M}}{4\pi\, r_J^2\, v(r_J)}. \tag{20}$$

The biconical geometry implies that the density diverges at the vertex. This does not present a practical problem, since the vertex also has vanishing volume for purposes of calculating the line flux.

The isovelocity zones for homologous expansion are well-known to be planes oriented to be normal to the viewer sightline (e.g., Mihalas 1978). Interestingly, the shapes defined by the intersection of such planes with the biconical flow geometry leads to conic sections, with the type depending generally on how the viewing inclination compares to the cone opening angle. For edge-on, the emitting surfaces are parabolae, with a gradient in surface brightness that drops quickly with height from the orbital plane.

The Doppler shift for a point in the jet as seen edge-on is

$$v_z = -\hat{z} \cdot \boldsymbol{v} + \Omega\, R_1 \sin(\varphi_b) \tag{21}$$

$$= -v_0 \frac{r_J \cos\theta}{R_1} + \Omega\, R_1\, \varpi_b \sin(\varphi_b) \tag{22}$$

$$= -(v_0/R_1) z + \Omega\, y + x_{bJ}, \tag{23}$$

where y and z are observer coordinates, and

$$x_{bJ} = \varpi_{bJ} \cos(\Omega t - \varphi_{bJ}). \tag{24}$$

Note that if the jet were not participating in orbital motion, the isovelocity zones would be planes normal to the observer sightline $\hat{z}$. The above expression reveals that for the biconical jet with homologous expansion, in conjunction with the solid body rotation (i.e., the biconical geometry is defined for the rotating frame), the isovelocity zones are still planar, but with a normal that is rotated with respect to $\hat{z}$. In the observer coordinates, the planes have normals, $\hat{n}$, with components:

$$n_x = \frac{\Omega\, R_1}{\sqrt{v_0^2 + \Omega^2 R_1^2}}, \tag{25}$$

$$n_z = \frac{v_0}{\sqrt{v_0^2 + \Omega^2 R_1^2}}. \tag{26}$$

The deviation of the isovelocity planes from having normals of the observer sightline $\hat{z}$ is given by $\cos\psi = \hat{z} \cdot \hat{n} = n_z$. The product $\Omega\, R_1 = 24\,\mathrm{km\,s^{-1}}$ is the speed of synchronous rotation at the equator of the Gainer. By contrast, one expects that $v_0 \sin\beta_J$ to approximately set the half-width of an emission line formed in the jet. For $\beta_J \sim 60°$ and the observed half-width around $300\,\mathrm{km\,s^{-1}}$, v_0 must be around $350\,\mathrm{km\,s^{-1}}$, demonstrating that the influence of solid body rotation is mild.

The Sobolev optical depth for a radial outflow in homologous expansion is

$$\tau_S = \mathcal{T}_J \left(\frac{\rho}{\rho_0}\right)^2 q(r), \tag{27}$$

where $\mathcal{T}_J$ is a line optical depth scale for the jet, and q is a function of radius that can subsume modifications to the recombination rate and other factors that alter the optical depth at Hα. Here, we use a power law, with $q \propto r^\delta$ as a way to make τ_S vary more or less steeply than ρ^2 with radius. The flux of line emission becomes

$$f_\nu(w_z) = \frac{1}{d^2} \int_{\varpi(w_z)}^{\infty} S_J (1 - e^{-\tau_S}) 4\alpha_0(r_J, v_z)\, r_J\, dr_J, \tag{28}$$

where S_J is the line source function for the jet. As with the disk, the jet is taken to be a source of blackbody radiation in the RJ-limit with temperature $T_J = 20{,}000$ K. For a spherical wind, $\alpha_0 = \pi/2$. For an edge-on biconical jet, α_0 is the half-opening angle of the parabolic isovelocity zone with observer impact parameter p. The factor of $4\alpha_0$ spans the full width of the upper and lower parabolae. Its value is given by the expression

$$\sin\alpha_0 = \sin\beta_J \sqrt{1 - \frac{p_{\min}^2(v_z)}{p^2}}, \tag{29}$$

where $p_{\min}$ is the impact parameter at the apex of the parabola as given by

$$p_{\min} = |z|/\tan\beta_J, \tag{30}$$

and $p = \sqrt{r_J^2 - z^2}$, for the isovelocity plane for which $z = R_1\, v_z/v_0$.

The effect of orbital motion is included for the line profile as follows. Since we have argued that modification to the isovelocity zones is rather small, we approximate the effect of orbital motion as a bulk velocity shift of the entire line shape by the amount:

$$\Delta v_z = +\Omega\, \varpi_{bJ} \sin(\Omega t + \varphi_{bJ}), \tag{31}$$

where the product $\Omega\, \varpi_{bJ}$ is the solid body rotation speed of the jet origin in the orbital plane, and φ_{bJ} is the azimuthal offset of the jet origin, about the barycenter, from the line of centers between the two stars.

The examples in the next section place the jet origin on the line of centers at the edge of the disk, for which $\varphi_{bJ} = 0°$ and $\varpi_{bJ} \approx 3.3$, so that $\Omega\, \varpi_{bJ} = 77\,\mathrm{km\,s^{-1}}$. We choose $\delta = 1$ giving $q \propto r$, and $v_0 = 150\,\mathrm{km\,s^{-1}}$.

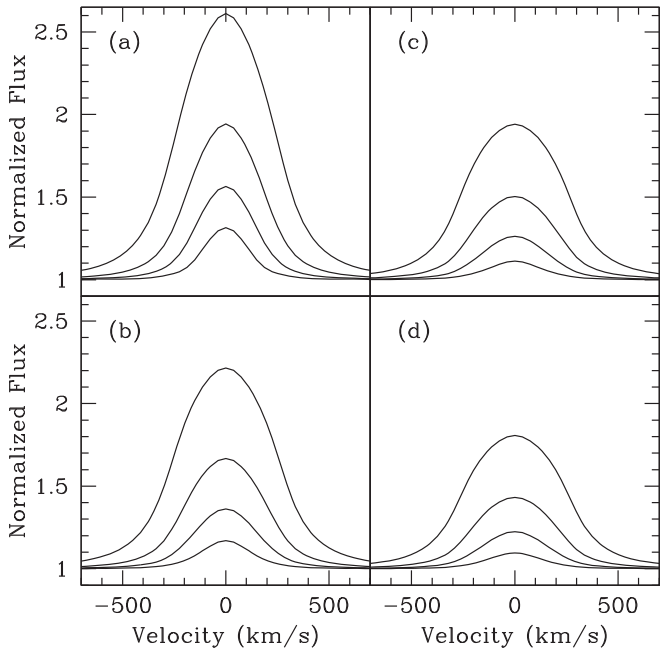

Figure 8. Series of model line profiles formed in the biconical jet with homologous expansion. Each panel has four line profiles, with $\mathcal{T}_L = 3.0$, 10.0, 30.0, and 100.0. The different panels are for different optical depths in the disk, with $\mathcal{T}_C = 0.3$, 1.0, 3.0, and 10.0 for panels (a)–(d), respectively.

3.2.2. Results

Figure 8 displays a sample of model line profiles for the biconical jet following the format for the disk case in Figure 6, and also evaluated at a phase of $\epsilon = 0.0$. The optical depth scale $\mathcal{T}_C = 0.3$, 1.0, 3.0, and 10.0 for panels (a)–(d), as in the

disk case. However, the four profiles are, with increasing line strength, $\mathcal{T}_L = 3.0$, 10.0, 30.0, and 100.0, which is different from the disk case.

Note that the jet model is distinct from the disk model in two particular ways. First, the disk is essentially truncated. In the orbital plane, its extent is limited by the presence of a binary companion. This is different from the expansive accretion disks that can form around pre-main-sequence stars (e.g., Isella et al. 2009). Vertically, the disk is limited by gravity and gas pressure-support. All else being equal, the line equivalent width for the disk grows slowly once the line becomes quite optically thick. In this regime, the line flux scales as a product of the projected area of the source and the source function, and the area is limited. On the other hand, although the jet is conical in angular extent, it is not limited in radial extent. Although unphysical, the line equivalent is formally unbounded in the model as $\mathcal{T}_L$ is increased.

Second, the jet does not easily produce a traditional P Cygni line profile (e.g., Lamers & Cassinelli 1999) because the jet is offset from the Gainer star. Typically, a jet seen at arbitrary inclination angle tends to produce a double-peaked line profile. If a jet originates from a star, then the outflowing portion directed toward the observer will also lie in front of the star, and so can produce the standard blueshifted absorption trough characteristic of a P Cygni line.[5] For β Lyr, the system is very close to edge-on. This means the line tends to be single-peaked instead of double-peaked. Being offset from the star means that when the jet is forward of the Gainer, then if there were no disk and if the system were edge-on, the absorption trough would be symmetric about line center, and a standard P Cygni line shape cannot result. Consequently, the model emission lines for the jet can grow to high peak values but are always single-peaked.

Figure 9 for jet lines with phase variations is similar to Figure 7 for the disk case. Each profile is for a different phase of the orbit, with $\epsilon = 0.0$ at the bottom, and $\epsilon = 1.0$ at the top. The slight modulation in location of the peak is the effect of orbital motion. The depression of the line emission at mid-phases is from the eclipse of the jet by the Loser star. Whereas the isovelocity zones for the disk were left–right symmetric so that the eclipse led to line asymmetry, the isovelocity zones for the jet are back-front symmetric in our model, and so the line profile remains symmetric about peak emission at all times.

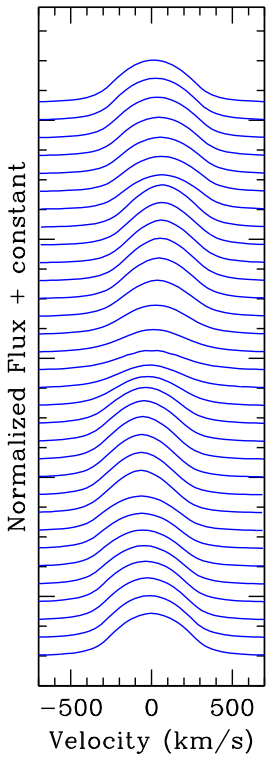

Figure 9. Series of jet line profiles with orbital phase for $\mathcal{T}_L = 100.0$ and $\mathcal{T}_C = 3.0$, following the style of Figure 7. The depression of the profiles around ϵ of 0.5 arises from an eclipse of the jet by the Loser. For this example, the jet is at the edge of the disk, on the line of centers for the two stars.

4. Discussion

Figure 10 shows a dynamic spectrum for the set of continuum-normalized Hα data. Spectra in the vicinity of Hα are displayed in phase order along the vertical, with velocity shift, relative to the rest wavelength of Hα, along the horizontal. The colors are for brightness, as indicated at far right. The dynamic spectrum shows two orbital phases, with the second being a repeat of the first, for ease of viewing. The lower panel gives an average spectrum for all the data.

The extension to large blueshift velocities well outside of Hα is shown because it captures an absorption feature from the atmosphere of the Loser star, shown as a black sinusoid. The full amplitude is approximately 400 km s^{-1}, twice the orbital speed of the Loser.

The Hα profile is complex. An FWHM is difficult to define, because the line shape is asymmetric and because the peak can vary significantly in value and velocity shift. Based on the average spectrum, the HWHM is around 225 km s^{-1}, with the line wings typically extending out to $\pm$400 km s^{-1}.

Peak brightness in Hα occurs around $\epsilon \sim 0$, which is when the Loser, which is the brighter component, is in eclipse. This certainly causes continuum-normalized line emission to increase because the continuum level for the binary is minimized. One might expect a similar brightening of Hα during secondary minimum around $\epsilon \sim 0.5$. Using the same data set as this paper, Gray & Ignace (2008) showed that the equivalent width of Hα is anticorrelated with the observed photometric light curve, and that the total line flux of Hα is roughly constant with phase, albeit with significant scatter. The significant brightening in the dynamic spectrum is approximately confined to $\Delta\epsilon \approx \pm 0.1$ in phase, which corresponds well to when the Loser is eclipsed by the disk, given the adopted geometrical parameters in Table 1.

One striking feature revealed by the dynamic spectrum is the blueshifted absorption. The feature appears somewhat prominently between phases of 0.1 and 0.4, then again less prominently from about 0.75 to 0.9. The feature has a width of about 50 km s^{-1}. For the lower phase interval, the feature appears to drift from about -150 to -50 km s^{-1}. For the higher phase interval, it drifts perhaps from -50 to -100 km s^{-1}, although it is unclear whether any drift occurs, owing to the weak level of absorption. Key is that the feature never moves to positive velocity shifts.

This component is clearly not ascribable to either the disk or jet, based on our qualitative modeling. While line asymmetry can result in the emission lines formed in the disk owing to

[5] Even for a recombination line that may not display a net absorption because the emission fills it in, one generally expects the blueshifted absorption to cause asymmetry in the line shape.

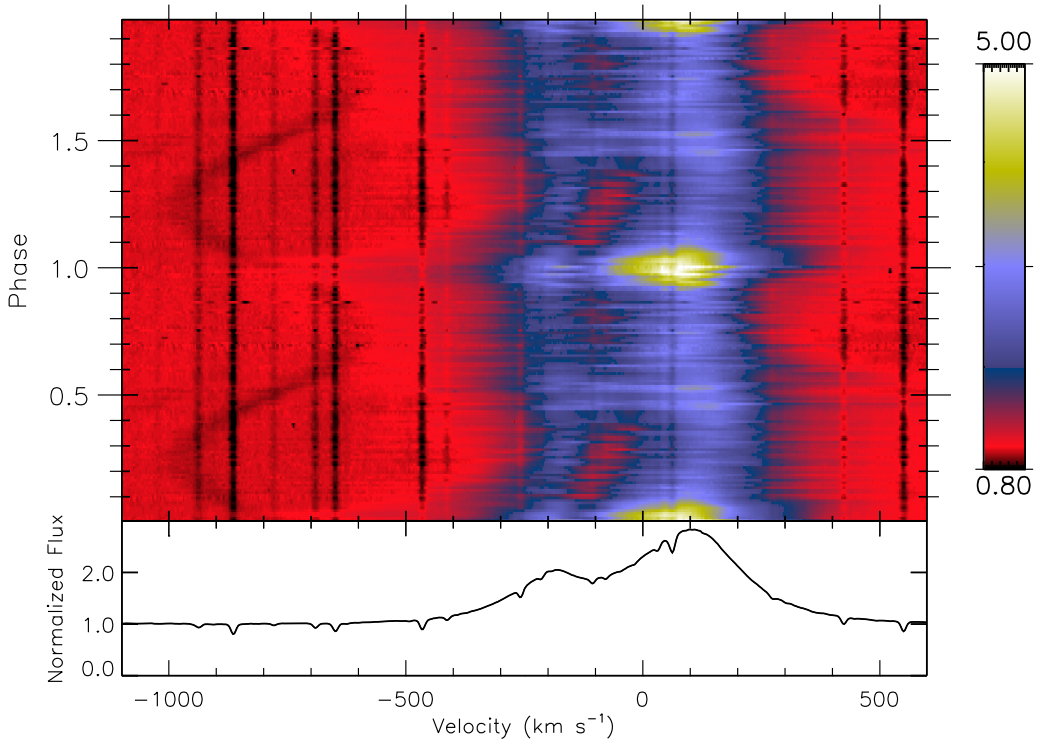

Figure 10. Dynamic spectrum for the phased continuum-normalized spectra in the vicinity of Hα. Bottom shows the average profile shape. A color scale for brightness is indicated on the right. The data in phase is repeated for ease of viewing. The sinusoid absorption feature in black centered near -800 km s^{-1} is associated with the Loser star.

eclipse by the Loser (cf. Figure 7), the effect drifts from blueshifts to redshifts (because the isovelocity zones are left–right symmetric), and is localized around $\epsilon \sim 0.5$, exactly where the observed component disappears. By contrast the line emission from the jet is always symmetric about the peak, even in eclipse, because the isovelocity zones are front–back symmetric. It is difficult to imagine how a detailed radiative transfer calculation involving both the disk and the jet plus the eclipse could produce the observed feature—its persistent blueshift and apparent drift—even if the disk and jet were nonaxisymmetric.

There are components in the β Lyr system that have not been considered in our modeling, such as a circumbinary envelope, a hot spot, and the accretion stream. We consider each of these in relation to the drifting blueshifted feature in the dynamic spectrum of Hα.

1. *Circumbinary Envelope:* A circumbinary envelope is likely to be a torus-like region residing outside of the binary as a whole. If rotating, its rotation must be slow. Treating the binary as a point source of mass with 16 $M_\odot$, the distance at which a rotation speed of 100 km s^{-1}, a value consistent with the feature, is achieved would be about 290 $R_\odot$, or roughly 5.2× the binary separation. There are several challenges for a circumbinary envelope explanation of the drifting feature. How would the feature avoid appearing at redshifted velocities? And why would it not be present for certain phase ranges?

   If the circumbinary torus were in expansion, then the feature might be explainable as a low-density segment of the torus. But then what is the origin for the nonaxisymmetry? The binary itself is the obvious choice. However, it seems challenging for any stationary structure (i.e., in the rotating frame of the binary) to avoid producing a feature at redshift velocities in the observer frame, as the source of asymmetry (e.g., if mass loss were to occur via the L2 and L3 points) would track with the binary orbit.
2. *Hot Spot:* Many authors suggest the presence of a hot spot where the accretion stream from the Loser lands at the accretion disk for the Gainer (e.g., Lomax et al. 2012). Consider a hot spot that is on the outer-facing rim of the vertically extended accretion disk, as a zone of limited arc along the rim. The spot is stationary in the rotating frame. For an edge-on observer, the spot is not viewable around $\epsilon \sim 0$ because of occultation by the disk, nor around $\epsilon \sim 0.5$ due to eclipse by the Loser star.

   A hot spot at the disk rim, as seen edge-on, would follow a velocity shift given by

$$v_z = -\Omega(R_D - \varpi_{b1})\sin(2\pi\ \epsilon). \tag{32}$$

   The corotation speed at the disk rim, from the barycenter, is $\Omega(R_D - r_{b1}) \approx 80$ km s^{-1}. The Keplerian rotation at the rim is about the same. The overall scale of these speeds at the hot spot is commensurate with the observed maximum blueshift value for the feature in Hα. Figure 11 illustrates how such a feature would migrate through a dynamic spectrum. Here the spot is eclipsed by the disk for orbital phases of 0.0–0.25, and then again for 0.75–1.0. It is also eclipsed by the Loser star at phase 0.5. For illustration purposes, the spot is simply assumed to be along the line of centers between the two stars. A hot spot produces a feature appearing at both blueshifted and redshifted velocities, which is not observed.

   For the mass transfer, one can imagine that the hot spot leads the Loser. This would mean that the spot appears before $\epsilon = 0.25$, and it would be eclipsed before

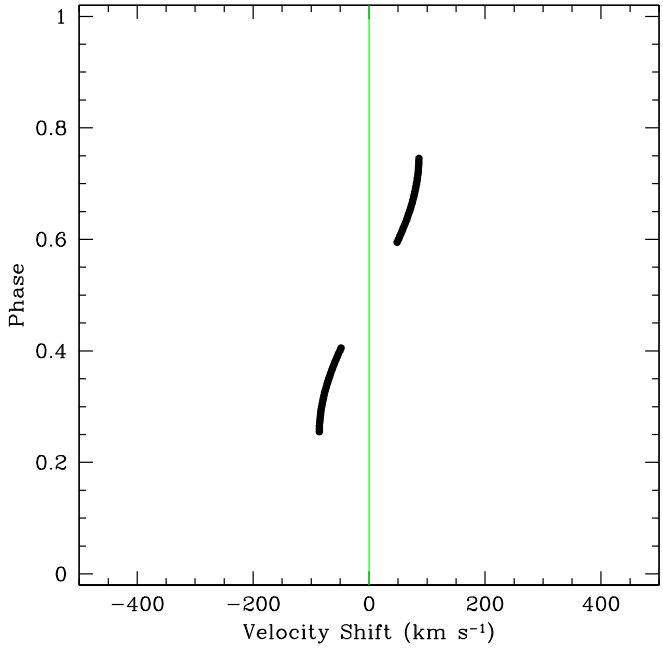

Figure 11. Displayed is the path of a "spot" on the disk (in emission or absorption) in velocity shift with phase. The spot is not seen at early or late phases when on the far side of the disk. The gap in the middle is when the spot is eclipsed by the Loser. See the text for further details.

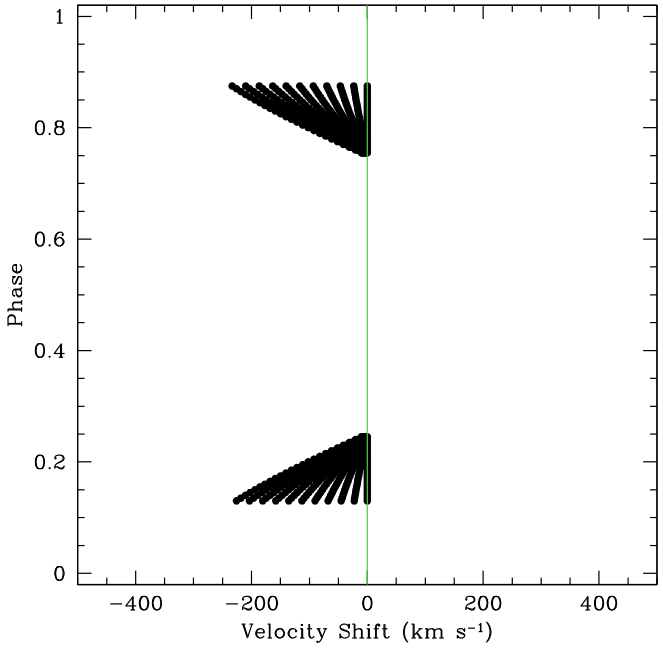

Figure 12. Displayed is the path of material in the accretion stream (in emission or absorption). The gap in the middle is when the origin of the accretion is blocked by the Loser. The gaps at early or late phases are when the Loser is eclipsed by the disk. The different lines are for different flow speeds in the stream. See the text for further details.

$\epsilon = 0.75$. Indeed, the geometry for a spot that leads the Loser in phase could allow for an eclipse that would largely block the spot by the Loser when at redshifted velocities. The challenge is that the spot would then be seen around $\epsilon = 0.5$, which is not observed. Furthermore, it seems almost impossible to understand how a spot could produce a blueshifted feature after $\epsilon = 0.5$.

3. *Accretion Stream:* For simplicity, imagine the accretion stream as a flow of material moving radially away from the Loser, along the line of centers joining the stars, to arrive at the accretion disk. This stream would be seen against the backdrop of the atmosphere of the Loser for phases below 0.25 and above 0.75. It would not be seen between phases of 0.25–0.75, as it would be blocked by the backside of the Loser. In addition, the stream would not be seen for phases of about 0.0–0.1 and 0.9–1.0, owing to occultation of the stream by the disk.

But when the stream is observed, it would be moving from the Loser toward the disk with a velocity component toward the observer, and so would appear strictly at blueshifted velocities, with $v_z = -v_{\rm acc}\cos(2\pi\ \epsilon)$, where $v_{\rm acc}$ is a free parameter for a stream of constant speed. Figure 12 shows how the kinematics of this feature would appear in a dynamic spectrum. The different lines are for different values of $v_{\rm acc}$. The lines replicate the overall observed pattern in Hα: the feature is blueshifted only, is absent at appropriate phase intervals, moves from high blueshifts to low ones as the Loser emerges from eclipse, and then when appearing again, the drift reverses to move from low to high blueshifts as the Loser moves toward ingress.

However, the observed feature is weaker at later phases than early phases. There are some possibilities for explaining this. The most plausible is that, like the hot spot concept leading the Loser, the accretion stream is probably curved. This would imply that the column of stream material is more lined-up with the observer sightline at early phases than at late ones. Such a detailed model is beyond the scope of this paper.

As plausible as this may seem, there is a severe challenge. The model so far neglects the contribution of the orbital motion for the kinematics of the stream. For early phases, the orbital motion adds a component of velocity toward the observer, thereby increasing the blueshifted speed. At late phases there is the addition of a redshifted component to the net Doppler shift. Figure 13 illustrates this effect.

Figure 13 is similar to Figure 12, with different curves for difference choices of $v_{\rm acc}$. A constant orbital speed of about $140\,{\rm km\,s^{-1}}$ has been included, with its phased-dependent velocity shift. The selected orbital speed is intermediate of the Loser's orbital speed of $180\,{\rm km\,s^{-1}}$ and that of the disk's rim at $80\,{\rm km\,s^{-1}}$. In addition, we allowed for the stream to be seen against the backdrop of the disk, as not all of the stream is eclipsed by the Loser between phases of 0.25–0.50.

The end result is that while the blueshifted portion of the curves can have approximately the right speeds at the correct phases, considerations of orbital motion result in the feature appearing at redshifts as well. If $v_{\rm acc}$ is small, the early phases can approximate the observations; however, at later phases the feature is entirely at redshifts. If $v_{\rm acc}$ is large, the feature still appears at redshifts for late phases, but also at low blueshifted speeds. However, high blueshift speeds are achieved at early phases, contrary to observations. Further detailed modeling is needed to determine if these shortcomings of the model can be overcome. Allowing for curvature of the accretion stream and acceleration of the accretion flow would certainly greatly alter the kinematical signature in a plot like Figure 13.

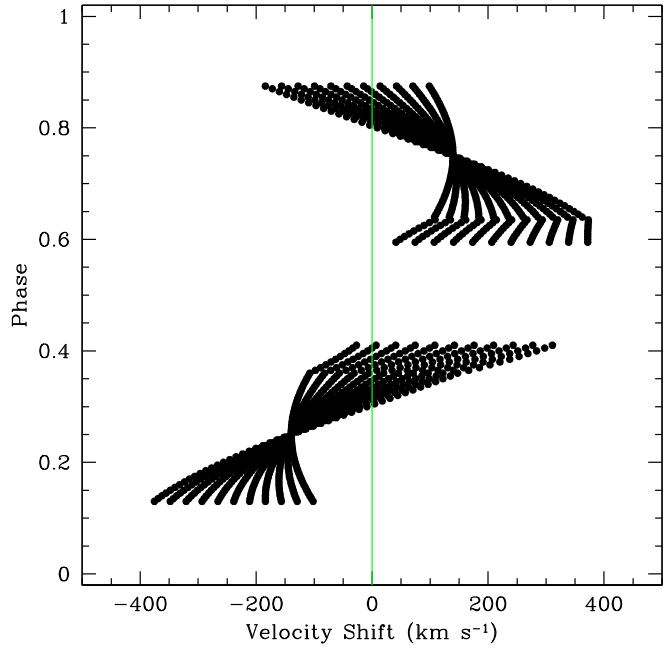

Figure 13. Similar to Figure 12, but now with orbital motion included. See the text for further explanation.

5. Conclusions

Further dedicated monitoring of the Hα emission line in β Lyr is needed to confirm suggestions that the well-known persistent blueshifted absorption feature at low velocity shifts in the line (a) does indeed come and go in certain phase intervals and (b) drifts in velocity. Hints of such effects have appeared in the literature. Honeycutt et al. (1993) also reported on a dynamic spectrum from a different data set and claimed to observe an "S-wave" feature of relative variation in the line profile with orbital phase. However, their data set had one-third as many spectra as this report, and their phase binning was more coarse. Using a subset of the archival data from Ritter, Ahmad & Zainuddin (2009) noted that the emission line can become single-peaked, indicating that the blueshifted feature does not exist for all phases.

Based on the data set described here, simplistic models were developed for emission lines formed in the disk alone or in the jet alone. Separately, these cannot produce the characteristic asymmetric double-peaked profiles. Evaluating the detailed radiative transfer for a model involving both a disk and a jet is unlikely to help. Using basic kinematical considerations, neither a circumbinary component (e.g., a "torus" in outflow or rotation), nor a hot spot seems capable of explaining the appearance and disappearance of the feature with phase or its migration in velocity shift. An accretion stream seems more promising, but also faces challenges. If new observations were to confirm the behavior of the feature as claimed here, the phase, velocity drift, and velocity width information is likely probing dense, asymmetric flow components in the system. Perhaps the magnetic field claimed to exist in the system, yet rather poorly understood, could prove relevant (e.g., Skulsky 2018).

The authors thank an anonymous referee for several helpful comments to improve this manuscript. The authors also gratefully acknowledge that archival data used for this paper and maintained by the University of Toledo Ritter Observatory is supported by the National Science Foundation Program for Research and Education with Small Telescopes (PREST). This research has made use of the SIMBAD database, operated at CDS, Strasbourg, France. This research has made use of NASA's Astrophysics Data System.

Appendix
Coordinate Transformations

The coordinate transformation between the observer system and that of the barycenter is given by the following sets of expressions, first for Cartesian coordinates:

$$\begin{pmatrix} x_{\rm b} \\ y_{\rm b} \\ z_{\rm b} \end{pmatrix} = \begin{pmatrix} \cos i & 0 & \sin i \\ 0 & 1 & 0 \\ -\sin i & 0 & \cos i \end{pmatrix} \begin{pmatrix} x \\ y \\ z \end{pmatrix}, \tag{33}$$

and for spherical coordinates:

$$\cos\chi = \cos\vartheta_{\rm b}\cos i + \sin\vartheta_{\rm b}\sin i\cos\varphi_{\rm b}, \tag{34}$$

$$\cos\theta_{\rm b} = \cos i\cos\chi + \sin i\sin\chi\cos\alpha, \tag{35}$$

$$\sin\chi\sin\alpha = -\sin\vartheta_{\rm b}\sin\varphi_{\rm b}, \tag{36}$$

$$\tan\alpha = -\frac{\sin\vartheta_{\rm b}\sin\varphi_{\rm b}}{\cos\vartheta_{\rm b}\sin i - \cos i\sin\vartheta_{\rm b}\cos\varphi_{\rm b}}. \tag{37}$$

The transformation from the barycenter to the coordinates of the Gainer is given by:

$$x_{\rm l} = x_{\rm b} - \varpi_{\rm b1}, \tag{38}$$

$$y_{\rm l} = y_{\rm b}, \tag{39}$$

$$z_{\rm l} = z_{\rm b}, \tag{40}$$

and

$$r_{\rm l}^2 = x_{\rm l}^2 + y_{\rm l}^2 + z_{\rm l}^2 \tag{41}$$

$$\cos\vartheta_1 = z_{\rm l}/r_{\rm l} \tag{42}$$

$$\varpi_1^2 = x_{\rm l}^2 + y_{\rm l}^2 \tag{43}$$

$$\tan\phi_1 = y_{\rm l}/x_{\rm l}. \tag{44}$$

The transformation from the barycenter to that of the Loser is quite similar, with the only difference being in the x-coordinate:

$$x_2 = x_{\rm b} + \varpi_{\rm b2}, \tag{45}$$

$$y_2 = y_{\rm b}, \tag{46}$$

$$z_2 = z_{\rm b}, \tag{47}$$

and

$$r_2^2 = x_2^2 + y_2^2 + z_2^2 \tag{48}$$

$$\cos\vartheta_2 = z_2/r_2 \tag{49}$$

$$\varpi_2^2 = x_2^2 + y_2^2 \tag{50}$$

$$\tan\phi_2 = y_2/x_2. \tag{51}$$

The coordinates for the jet system are defined in terms of the Gainer coordinates. The $+x$-axis for the jet coordinates is along the outward cylindrical radial to the jet from the Gainer, $+\hat{\varpi}_{1J}$. The z-axis for the jet is parallel to that of the Gainer, and so the y-axis for the jet is defined by $\hat{z}\times\hat{x}$. If the vertex of the jet is oriented in the disk plane at azimuth φ_{1J}, then the Cartesian

coordinate transformation is given by:

$$\begin{pmatrix} x_1 \\ y_1 \\ z_1 \end{pmatrix} = \begin{pmatrix} \cos\varphi_{1J} & \sin\varphi_{1J} & 0 \\ -\sin\varphi_{1J} & \cos\varphi_{1J} & 0 \\ 0 & 0 & 1 \end{pmatrix} \begin{pmatrix} x_J + \varpi_{1J} \\ y_J \\ z_J \end{pmatrix}, \quad (52)$$

ORCID iDs

Richard Ignace https://orcid.org/0000-0002-7204-5502
Derck Massa https://orcid.org/0000-0002-9139-2964

References

Ahmad, N., & Zainuddin, Mohd, S. , M. Z. Y. 2009, in ASP Conf. Ser. 404, The Eighth Pacific Rim Conference on Stellar Astrophysics: A Tribute to Kam-Ching Leung, ed. B. Soonthornthum et al. (San Francisco, CA: ASP), 297
Alduseva, V. Y., & Esipov, V. F. 1969, SvA, 13, 83
Appenzeller, I., & Hiltner, W. A. 1967, ApJ, 149, 353
Batten, A. H., & Sahade, J. 1973, PASP, 85, 599
Bisikalo, D. V., Harmanec, P., Boyarchuk, A. A., Kuznetsov, O. A., & Hadrava, P. 2000, A&A, 353, 1009
Bonneau, D., Chesneau, O., Mourard, D., et al. 2011, A&A, 532, A148
Etzel, P. B., & Meyer, D. M. 1983, PASP, 95, 891
Gray, S. K., & Ignace, R. 2008, JSARA, 2, 71
Hack, M., Hutchings, J. B., Kondo, Y., et al. 1975, ApJ, 198, 453
Harmanec, P. 2002, AN, 323, 87
Harmanec, P., Morand, F., Bonneau, D., et al. 1996, A&A, 312, 879
Harmanec, P., & Scholz, G. 1993, A&A, 279, 131
Hoffman, J. L., Nordsieck, K. H., & Fox, G. K. 1998, AJ, 115, 1576
Honeycutt, R. K., Turner, G. W., Vesper, D. N., Robertson, J. W., & White, J. C., II 1993, PASP, 105, 426
Horne, K., & Marsh, T. R. 1986, MNRAS, 218, 761
Huang, S.-S. 1963, ApJ, 138, 342
Huang, S.-S. 1978, ApJ, 222, 627
Hubeny, I., Harmanec, P., & Shore, S. N. 1994, A&A, 289, 411
Hubeny, I., & Plavec, M. J. 1991, AJ, 102, 1156
Ignace, R. 2010, ApJ, 725, 1040
Ignace, R., Oskinova, L. M., Waldron, W. L., Hoffman, J. L., & Hamann, W.-R. 2008, A&A, 477, L37
Isella, A., Carpenter, J. M., & Sargent, A. I. 2009, ApJ, 701, 260
Jameson, R. F., & King, A. R. 1978, A&A, 63, 285
Jameson, R. F., & Longmore, A. J. 1976, MNRAS, 174, 217
Knappenberger, P. H., & Fredrick, L. W. 1968, PASP, 80, 96
Kondo, Y., McCluskey, G. E., Silvis, J. M. S., et al. 1994, ApJ, 421, 787
Lamers, H. J. G. L. M., & Cassinelli, J. P. 1999, Introduction to Stellar Winds (Cambridge, UK: Cambridge Univ. Press), 452
Leone, F., Plachinda, S. I., Umana, G., Trigilio, C., & Skulsky, M. 2003, A&A, 405, 223
Linnell, A. P. 2000, MNRAS, 319, 255
Linnell, A. P. 2002, MNRAS, 334, 963
Lomax, J. R., Hoffman, J. L., Elias, N. M., II, Bastien, F. A., & Holenstein, B. D. 2012, ApJ, 750, 59
Mazzali, P. A. 1987, ApJS, 65, 695
Mazzali, P. A., Pauldrach, A. W. A., Puls, J., & Plavec, M. J. 1992, A&A, 254, 241
Mennickent, R. E., & Djurašević, G. 2013, MNRAS, 432, 799
Mewe, R., Heise, J., Gronenschild, E. H. B. M., et al. 1976, Ap&SS, 42, 217
Mihalas, D. 1978, Stellar Atmospheres (2nd ed.; San Francisco: Freeman)
Nazarenko, V. V., & Glazunova, L. V. 2003, ARep, 47, 1013
Nazarenko, V. V., & Glazunova, L. V. 2013, ARep, 57, 294
Rucinski, S. M., Pigulski, A., Popowicz, A., et al. 2018, arXiv:1803.10569
Rybicki, G. B., & Hummer, D. G. 1978, ApJ, 219, 654
Rybicki, G. B., & Hummer, D. G. 1983, ApJ, 274, 380
Sahade, J. 1980, SSRv, 26, 349
Sanyal, A. 1976, ApJ, 210, 853
Schmitt, H. R., Pauls, T. A., Tycner, C., et al. 2009, ApJ, 691, 984
Skulskij, M. Y. 1982, SvAL, 8, 126
Skulsky, M. Y. 2018, CoSka, 48, 300
Sobolev, V. V. 1960, Moving Envelopes of Stars (Cambridge, MA: Harvard Univ. Press)
Umana, G., Leone, F., & Trigilio, C. 2002, A&A, 391, 609
Wade, C. M., & Hjellming, R. M. 1972, Natur, 235, 270
Wilson, R. E. 1974, ApJ, 189, 319
Zeilik, M., Heckert, P., Henson, G., & Smith, P. 1982, AJ, 87, 1304
Zhao, M., Gies, D., Monnier, J. D., et al. 2008, ApJL, 684, L95